



Biomechanical Aspects of *in Vitro* Fertilization

Liliya Batyuk¹, Anatoly Khalin², and Natalia Kizilova³✉

¹ Kharkiv National Medical University, Nauki 2, Kharkov 61022, Ukraine

² Kharkiv National University, Svobody 4, Kharkov 61022, Ukraine

³ Warsaw University of Technology, Nowowiejska 24, 00-665 Warsaw, Poland

Abstract. During the last decades, *in vitro* fertilization (IVF) became one of the most demanded reproductive technologies used for infertility treatment. Despite the significant efforts, the percentage of successful procedures remains moderate (<50%). It is shown, the percentage of successful IVF could be increased by a patient-specific embryo transfer based on the preliminary biomechanical and CFD analyses. A detailed review on different aspects of the IVF procedure is given. CFD simulations on the embryo transfer with tubular fluid and air bubble through a thin rigid tube (catheter) have been carried out. The following parameters were found to be the most influencing on the embryo transfer to the fundus: (i) the injection time IT, (ii) the distance of the catheter tip to fundus; (iii) the injected volume during the first stage; (iv) duration of the second stage; (v) the withdrawal speed at which the catheter is removed at the last stage; (vi) the volume replacement during catheter withdrawal. The IT, catheter load speed and cumulative shear stress over the particle during the IT were found the main prognostic factors of the IVF success.

Keywords: In vitro fertilization (IVF) · Embryo · Viscoelasticity · Damage · Computational fluid dynamics

1 Introduction

In vitro fertilization (IVF) is one of the widely known types of assisted reproductive technologies that includes artificial fertilization of the preliminary collected eggs, their culture during 4–6 days and further embryo transfer (ET) and its implantation into the uterus. The success of the IVF is estimated by the pregnancy rate (PR) that significantly depends on the age and a series of other factors of the women; it varies between PR = 39.6% at the age <35 to PR = 11.5% at the age >40 [1]. Mechanical factors play an essential role in cell divisions and embryo development [2], locomotion and invasion [3], differentiation [4], mechanotransduction [5], apoptosis [6], cell proliferation, gene and protein expression [7, 8]. Any variations in the mechanical environment influence the mechanical tension within the cytoskeleton of living cells that is a critical regulator of their biological function [5, 7], that will ultimately affect the respective functionalities. Mechanical inputs play a major role in regulating cell fate and function at the molecular level [9], and a cell's internal state is also reflected in its mechanical properties like elasticity, viscosity and dielectric coefficients [10–13].

During the last decade, the following aspects of IVF have been intensively discussed in literature [14–22]:

- 1) estimation of mechanical factors crucial for successful IVF and ET;
- 2) elasticity and viscosity of the embryo as indicators of its state and development;
- 3) microfluidic systems for embryo development at dynamical mechanical conditions;
- 4) development of robotic assisted equipment for IVF, embryo development and ET;
- 5) elaboration of the patient specific technique of ET.

2 Biofluid Mechanics of Reproduction

2.1 Mechanical Properties of Embryos

Each fertilized egg (oocyte) develops through the following stages: (I) morula, when cells have rapidly mitotically divided to produce a solid mass of 12–15 cells; (II) blastula or blastocyst that consists of an outer layer, an inner cell mass and a fluid-filled cavity; (III) blastocyst hatching (i.e. lost of the zona pellucid (ZP) which is a specialized extracellular matrix surrounding the developing oocyte within the ovary) followed by its free floating; (IV) implantation into the fundus. Structure and mechanical properties of the embryo at the stages I–IV differ significantly.

ZP (Fig. 1a) forms a multilaminar spherical shell of remarkably uniform thickness (5–10 μm) and a negligible flexural rigidity [23] that plays an essential role in both natural and *in vitro* fertilization [24]. ZP is a glycoprotein gel that can be modeled as viscoelastic Maxwell body [25]. The oocyte is free of residual membrane stress and after compression it recovers its initial shape with no residual deformations. The mechanical parameters of the oocyte and ZP can be measured in micropipette experiments (Fig. 1a). Embryo and oocyte stiffnesses are correlated, indicating that there may be a link between mechanics and viability [26–28].

After fertilization the mean Young's modulus of the ZP demonstrates a 1.8–2.4-fold increase preventing the oocyte from polyspermy [23, 29]. Starting from the 8-cell stage with cell divisions and gradual transition to the morula stage, ZP gradually softens again allowing further enlargement of the embryo [27, 28]. Therefore, the Young's modulus of the ZP at different stages are known from the aspiration tests and some microfluidic experiments [3, 19, 22]. It was shown, the aged mice oocytes are significantly softer and demonstrate bigger relaxation times than the young oocytes [30]. Elastic modulus (E) and apparent viscosities (η) of the embryo cells at the stages I, II, III were measured as $E = (0.9 \pm 0.4; 0.4 \pm 0.2; 0.4 \pm 0.1)$ kPa and $\eta = (166 \pm 81; 77 \pm 37; 40 \pm 15)$ Pa \cdot s accordingly [31]. The embryos are very sensitive to mechanical properties of the substrate, i.e. the elasticity of the culture environment and the forces exerted over their surface. At the natural conditions, the stiffness of the uterine epithelium is ~ 1 kPa. Normally developed and damaged embryos are mechanically more strength than the damaged ones with blastomere fragmentation [32]. It was shown, the viability of the embryo at the 4-cell stage can be predicted with 90% sensitivity and 91% specificity based on the combination of mechanical (E_1, η_1) and two cell cycle parameters.

Based on the measurement data, several theoretical models of the embryo with ZP as an elastic incompressible half-space (half-space model), an elastic compressible bilayer

(2-layered model), and an elastic compressible shell (shell model) have been proposed [23]. The experimental studies with micropipette shown the layered and shell models are more precise. An equivalent rheological model as a modification of the Zener viscoelastic body (Fig. 1b) with, $E_1 = 0.3 \text{ N/m}$, $E_2 = 0.12 \text{ N/m}$, $\eta_2 = 0.59 \text{ N} \cdot \text{s/m}$ has been proposed in [33].

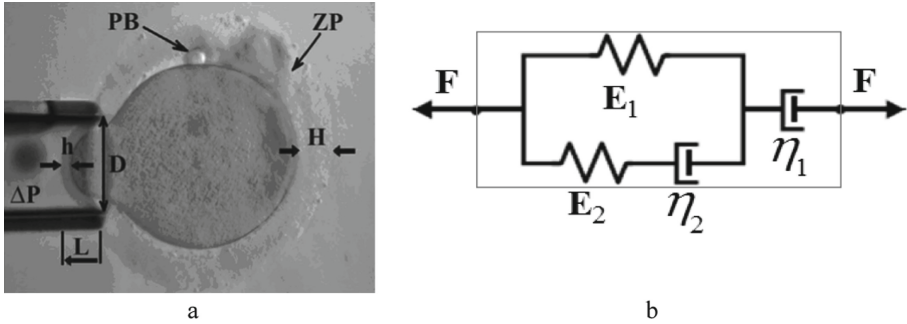


Fig. 1. Aspiration of the oocyte into a micropipetter (a) and its rheological model (b); H and h are the thickness of ZP outside and inside the pipette with inner diameter D, ΔP is applied negative pressure; L is the aspiration length, $E_{1,2}$ and $\eta_{1,2}$ are elastic and viscous moduli.

2.2 Peristaltic Wave Propagation and Oscillatory Fluid Dynamics

Fluid dynamics aspects of the embryo development are connected with permanent fluid motion in the oviduct and uterus due to their smooth muscle contraction and beating of the ciliated epithelial cells [34]. Their importance was examined both experimentally and theoretically and different mechanical and electric properties of the tubular, ampulary and isthmic fluids have been shown [34, 35]. The embryo movement along the oviduct to the fundus is provided by ciliary beating of the epithelial cells; contraction of the smooth muscle; flows of the fluids secreted; thermotaxis due to the temperature differences ($\sim 0.02 \text{ C}$) in different parts of the uterus.

Cilia beating generate a continuous fluid stream that extends up to $\sim 0.5 \text{ mm}$ over the tips of the cilia. Therefore, it is highly probable that the embryos are not moved by a cilia stroke directly acting upon them but by the continuous fluid flow generated by the cilia beating with frequencies $f = 5\text{--}20 \text{ Hz}$ [36]. The embryo transportation can be conducted by both direct contact of the moving cilia with its surface and by the drag force ($\sim 1.1 \cdot 10^{-9} \text{ N}$) produced by the fluids accelerated by the cilia contractions [37]. The cilium beat has the following characteristics: (i) its rate is remarkably uniform, and (ii) the beat of a particular cilium and its adjacent cilium appears to be well coordinated and generate a wave with the period $\sim 2.5 \text{ s}$ and length $\lambda \sim 500 \mu\text{m}$ [38]. The decreased ciliation and low cilia beat frequency are observed in women with obstructive tubal infertility [39]. The mechanics of viscous-dominated microscale flow *in vivo*, including time-reversal symmetry, drag anisotropy of slender bodies, and wall effects have been reviewed in [40]. Therefore, in the oviduct the embryo is subjected to the following dynamical forces [41]:

- 1) shear stress produced by tubal fluid flow;
- 2) compression by peristaltic tubal wall movement;
- 3) buoyancy due to differences in the density;
- 4) kinetic friction forces between the embryo and cilia.

All the factors lead to an average ovum velocity $\sim 0.1 \mu\text{m/s}$ that can be increased to $3.8\text{--}6.8 \mu\text{m/s}$ by smooth muscle contraction of the walls. Fluid movements produced by wall peristalsis are similar to those induced by beating cilia and reach an average velocity of $\sim 8.6 \mu\text{m/s}$ [36]. The motion of the embryo along the oviduct is not uniform. At some stages and conditions it could be accelerated or decelerated and even stopped by the active embryo-maternal interactions to provide the needed maturation of the embryo before delivering it to the fundus [42].

Based on the data that *in vivo* an embryo is naturally exposed to constant vibrations of ~ 6 Hz with the gradual increase to ~ 20 Hz, a new approach to *in vitro* culture of human embryos with natural type mechanical micro-vibrations has been proposed [41]. It was shown, in the group of patients who underwent the IVT of the embryo(s) grown *in vitro* under mechanical vibrations the pregnancy rate was higher.

2.3 Mathematical Modeling of the Natural Embryo Transportation

In earlier analytical studies (1965–1985) simplified models has been elaborated, including infinite symmetric circular channels, inviscid fluids, small-amplitude oscillations, infinite wavelength, and elastic walls. Later studies accounted for the finite-length nonuniform channels, viscous fluids, non-steady low Reynolds number flows, finite wavelength and viscoelastic wall [34, 43, 44] and peristaltic flows of non-Newtonian viscoelastic fluids [45]. A 2D rectangle and tapered channel models with the walls oscillated sinusoidally with a phase shift $\Delta\varphi$, have been developed and solved based on the lubrication theory [46]. It was shown, the transport phenomena are strongly affected by $\Delta\varphi$. A two-layer flow with an inner layer through which the egg moves was coupled with an outer layer through which flow is assumed to be driven by the pressure gradient only [47]. The ciliary sublayer at the interface of the inner and outer layers was modeled by a distribution of volume forces produced by the cilia beating and muscle contraction.

A stochastic model of ovum transport based on Langevin's diffusion equation was proposed in [48]. The embryo motion was considered as one-dimensional random walks in a field of external force that included ciliary beating, smooth muscle contractions and the frictional force produced by the viscous fluid. The model predicted the leading role of cilia activity in fast transport of the embryo.

For Stokes flow, the grid-free method of regularized Stokeslets that restores the flow field from a distribution of regularized forces supported by the immersed boundary can be used. The models of cilia beating [34], peristaltic pumping of solid particles [34], and 3d swimming [49, 50] have also been studied based on the immersed boundary method (IBM). The coupling between the wall movement and the fluid flow can be described as a fluid-structure interaction (FSI) problem and solved by the IBM, finite element (FEM) and finite volume (FVM) methods. Nowadays the FSI modeling and FEM simulations is the most popular approach to the embryo transportation problem *in vivo* and *in vitro*.

2.4 Biomechanical Aspects of IVF

In vitro ET remains the most inefficient step in IVF procedure and limiting component to its success rate [51]. While fertilization in the laboratory is achieved at relatively high success rates (>90%), the maximum chance of pregnancy per cycle is <20% in healthy couples [52]. Only top clinics report PR >40%, while others have PR <10% and even in developed countries the number of clinics with a low PR is very high. Depending on the IVT technique, a pregnancy rate of 33.3% is considered as excellent transplantations and 10.5% as poor ones. Among other hypotheses, it was suggested that mechanical factors, such as catheter type, method of loading the catheter, placement of the catheter tip and injection speed (IS) may be the cause for the low PR. Therefore, methods to improve the effectiveness of ET are needed. The IS, the time between the end of the injection and the catheter withdrawal, the withdrawal speed are important fluid dynamics parameters that may have an effect on the result of the ET procedure [53].

Standard IVT procedure starts with a proper positioning of the patient, proper positioning of the catheter in the uterine cavity (Fig. 2a) under guidance of abdominal ultrasonography (USG). Then, the inner catheter with a soft tip preliminary loaded with the embryo(s) is placed inside the outer one by the laboratory technician or embryologist. The ‘3-drop technique’ when a drop of medium (Embryo-Glue®) containing the embryo is separated from a preceding and following drops by air bubbles (Fig. 2b) is commonly accepted [54]. The air bubbles are visible by USG and serve as markers for correct embryo’s placement in the uterus. To minimize the risk of retained embryos, the catheter should be slowly withdrawn. Nevertheless, there is no unified point of view on the recommended times and speeds of the withdrawal.

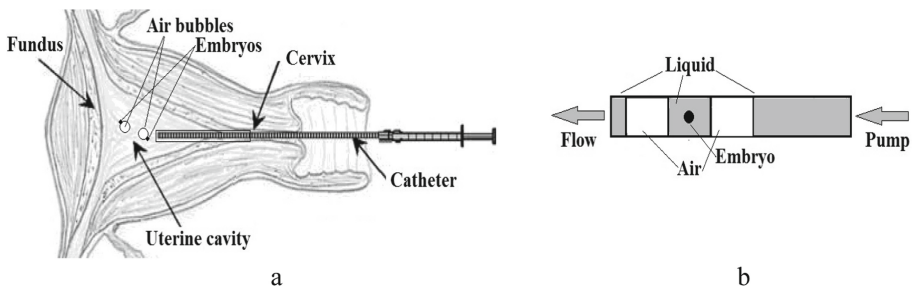


Fig. 2. Scheme of the embryo transfer (a) and the catheter tip loading (b)

2.5 Experimental studies on the uterine models

The IVT procedure with a loaded catheter (Fig. 2b) has been reproduced on a glycerin-filled rigid transparent model that imitated the inner cavity of the uterus (Fig. 3a). The model was installed on a plate inclined between 0–30° above the horizontal plane to repeat possible orientations of the uterus during the real ET procedure [55]. The transferred liquid was colored with a dye and its injection was recorded by a video camera. An example of the recording is given in Fig. 3b.

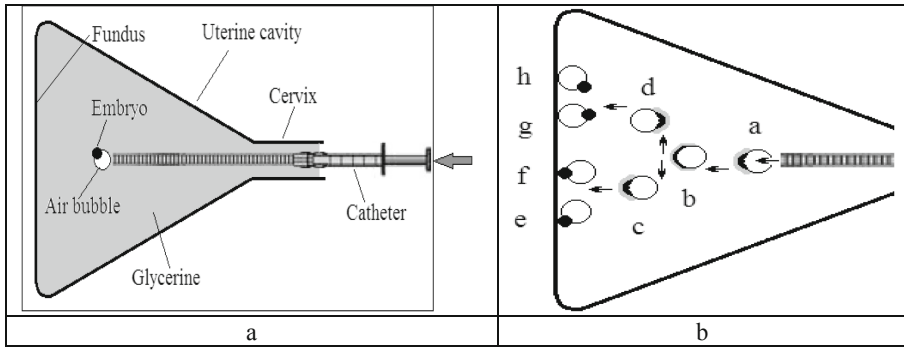


Fig. 3. A scheme of the experimental model for the laboratory simulations of ET (a) and possible trajectories of the bubbles with embryos (black) and transported liwuid (grey); e, f and g, h are successful and unsuccessful locations of the bubbles at the fundus.

As it was shown in the experimental studies on the model, its inclination angle influences the bubble formation and transportation of the embryo in the transferred fluid together with the bubble to the fundus via influencing the buoyancy forces [55]. Thus, the ET procedure must be performed at a patient-specific position in which the fundus location is exactly ahead of the buoyancy-driven trajectory of the bubble. In *in vivo* conditions this trajectory will also be influenced by the active oscillatory forces produced by the soft tissues and fluid flows, that makes the decision making much more difficult. It was demonstrated that the air bubbles did not move after immediate ambulation after transfer in 94.1% of the cases [56] which means the fluid dynamics of the IVT is still poor understood.

It was confirmed that the underlying dynamics of the ET highly depends on the individual uterine anatomy (size, inclination angle), type and location of the catheter, the injection and catheter withdrawn parameters (timings and speeds); the relationship between all the factors are not well understood.

2.6 Catheter Tip Location

As it was reported in many papers, placement of the tip of the catheter in the middle of the uterine cavity resulted by higher PR [57]. In different studies the best location of the catheter tip is described as 0.5–2 cm from the fundus [57, 58]. When the catheter tip is placed close to the fundus (<5 mm), IR decreases. As it was shown in a detailed study based on 5055 US-guided ET [59], the PR is higher when the embryos are injected at some distance >10 mm from the fundus. Recently it was shown the embryo(s) must be released at 5–15 mm from the fundus [60]. The PR were 65.2%, 32.2% and 2.6% when the catheter tip was located at the distance <10 mm, 10–20 mm, and 20 mm, respectively [61].

2.7 Ejection Speed and Duration

Catheter ejection speed influences depth and placement of the embryo into the uterine cavity [62]. Nevertheless, the speed of injection is not defined in the public protocols;

it is just generally advised to do the ET very gently/slowly [58]. Despite numerous experimental studies on the best injection speed for successful ET, a large variation in PR rates 26–40% is observed among laboratory technicians [63]. The measurements of the speed and duration of the ejection conducted by 7 technicians revealed the differences from $v = 2\text{--}4$ m/s and $T = 100$ ms to $v = 0.1\text{--}0.2$ m/s and $T = 750\text{--}1500$ ms [63]. As it was shown in the experiments on the rigid transparent model of uterus [55], the injection speed significantly influences the air bubble formation and transportation together with the embryo(s). The minimal delivering time $t > 10$ s was proposed. An automated pump-regulated embryo transfer (PRET) unit has been proposed for standardization of the ET procedure [62, 63]. The pump applies the constant pressure to a syringe connected with the catheter and, therefore, provides a patient-specific constant speed of ejection. A randomized controlled trial conducted on 599 IVT procedures has shown, the PRET device generates a significantly smaller variance of the positioning of the embryo(s) into the uterine cavity that resulted in an ongoing PR = 21% in the PRET versus 17% in the manual ($p = 0.22$) transfer groups.

The patient specific hydraulic resistance of the uterine cavity must be accounted for but there are still no reliable experimental data on uterine resistance in ET [62].

2.8 Fluid Composition and Viscosity

The transfer media for ET are elaborated and manufactured by different pharmaceutical companies and have different compositions. One of the most important natural macromolecule recommended to be introduced into the media is hyaluronic acid (HA) that is an implantation enhancing-molecule [64]. EmbryoGlue® is a useful and available ET medium with a high concentration of HA. In the model studies the viscosity of the transfer media is often considered as equivalent to that of water, while the individual viscosity of human uterine fluid is not measured, though it is believed to be much higher. As it was shown on the laboratory model [55], better dispersion of the air bubbles with embryo(s) is achieved when the viscosity of the transfer media is close to that of the uterine fluid.

3 Mathematical Modeling of the Embryo Transfer

Individual anatomical features of the uterine cavity (size, geometry, inclination angle, presence of fibroids and other deformations) are important factors for the ET procedure [65]. Therefore, CFD simulations on the patient-specific models may provide the optimal biomechanical details of the ET for the individual patient. FSI modeling and CFD computations of ET have been carried out on a 2d model of uterus as a fluid-filled thin open ends channel with a rigid catheter inside (Fig. 4) [66]. The effects of uterine peristalsis on ET during and after injection have been investigated by the wall movements. The fluid flow was governed by incompressible Navier-Stokes equations. The peristaltic flow was generated by the transverse sinusoidal displacement of the walls with period T and phase shift φ in the form

$$\begin{aligned} H_1(t, x) &= b \cos(2\pi(x/\lambda - t/T) - \varphi/2) - a, \\ H_2(t, x) &= b \cos(2\pi(x/\lambda - t/T) + \varphi/2) + a. \end{aligned}$$

The injection speed from the catheter tip was $U_{inj} = KU \sin(2\pi t/T_{inj})$, where U is the speed of the wave, $K = \text{const}$, $T_{inj} = T/2$ is the IT.

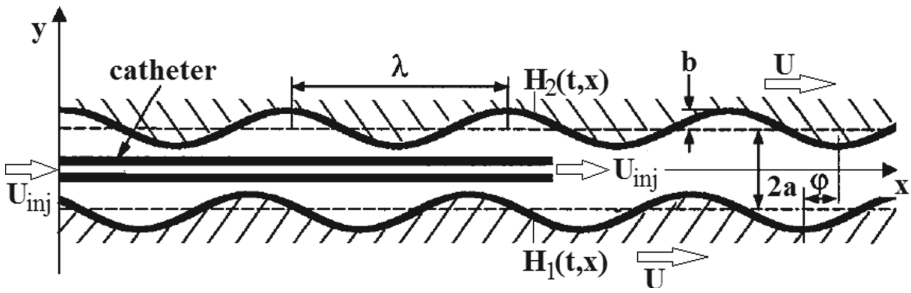


Fig. 4. The 2d model of ET into a channel with oscillating walls (from [66]).

It was shown, the displacement of the embryos as massless particles significantly depends on their location in the catheter (at $y/R = 0, 0.25, 0.5$ or 0.75 , where R is the inner radius of the catheter). The central positions lead to the longer axial transfer of the particle, while any large distortion of the particle leads to the large amplitude radial displacements. The performed CFD studies revealed that higher injection speed of the particles located at $y/R = 0$ moves the embryo farther toward the fundus. The viscosity of the human uterine fluid was taken from the experimental measurements on animals $\mu = 1 \text{ Pa} \cdot \text{s}$.

Peristaltic flow in a 2d tapered tube model of uterus with oscillating walls and a rigid catheter along its axis was also studied [46]. The influence of the IT, the catheter distance from the fundus, the injected volume, the rest time, the withdrawal speed and the volume replacement generated by the catheter withdrawal has been modeled. Based on the CFD data, the risk function of the unsuccessful ET and the ectopic pregnancy as a linear combination of the average distance to the fallopian tubes, and location of the embryo relatively to the fundal wall was proposed.

A 3d uterine model as an axisymmetric tube with periodical varying cross-sectional area with a closed end (Fig. 5) was studied in [49, 50]. It was shown, the embryo trajectories are strongly affected by the damping out the peristaltic wave towards the end, and the trajectories of a particle of finite volume differ from the trajectories of massless particles. When initial location of the embryo was closer to the wall (far from the axis) the particles got scattered by the fundus and returned back to the catheter.

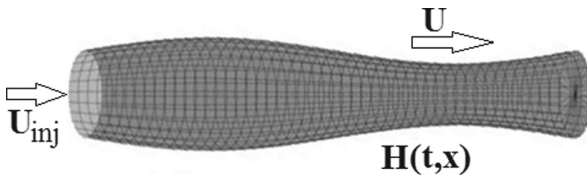


Fig. 5. 3d axisymmetric tube model of the uterine cavity (from [50]).

Based on the reviewed literature, the following essential biomechanical problems of IVF and ET can be formulated for improvement of the technique and increasing the PR:

- 1) Mathematical modeling of the ET along the inner tube between two air bubbles with embryo as a viscoelastic particle with different elastic and viscous coefficients (Fig. 2b);
- 2) Mathematical modeling of the ET between two air bubbles inside the model of uterus (both rigid and soft contracting walls);
- 3) Accounting for patient-specific geometry of the uterus (size, shape, antverted/retroverted/midposition) that influences the buoyancy forces acting onto the air bubbles and the embryo movement between them;
- 4) Computer simulations of the ET with different size/location of the bubbles and medium aimed at proper embryo delivery and minimization the risk of retained embryos.

4 Mathematical Problem Formulation

Steady flow of two air bubbles (Fig. 6) of the length 7 mm in the polyethylene tube with $D = 2R = 0.55$ mm inner diameter with a column of the Embryo-Glue® fluid of the length 52 mm in between them is considered. The total length of the composition $L = 83$ mm. The IT is ~ 20 s, so the average injection velocity $U_{inj} \sim 4$ mm/s. For the comparative analysis the velocities $U_{inj} = 1; 5; 20$ mm/s have been chosen. These values correspond to the IT = 80; 17; 4 s. To avoid the influence of the entrance and exit flows on the flow parameters, the longer tubes of $L = 15\text{--}30$ cm will be considered.

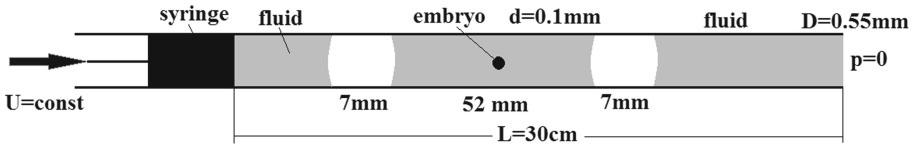


Fig. 6. A sketch of the modeled flow (the explanations are in the text).

The mathematical problem formulation for the multiphase flow is described by the steady Navier-Stokes equations [67]

$$\begin{aligned} \nabla \cdot v &= 0, \\ \rho v \cdot \nabla v &= -\nabla p + \mu \Delta v \end{aligned} \quad (1)$$

with the boundary conditions at the bubble surface S_b

$$n \cdot T = \frac{1}{Ca} \left(\frac{d\tau}{ds} + \frac{n}{r} \frac{dz}{ds} \right) - p_a n, \quad (2)$$

where n and τ are unit normal and tangent vectors at the point of the surface, p_a is the excess pressure inside the bubble, $T = -pI + (\nabla v) + (\nabla v)^T$,

$$z = 0 : \quad T_{zz} = -p_{in}, \quad r = 0 : \quad T_{zr} = -0, \quad r = 0 \cup S_b : \quad n \cdot v = 0. \quad (3)$$

Solution of the problem (1)–(3) has been obtained by the finite element method and Ansys Fluent 19.2 for the multiphysics flows at low Reynolds numbers $Re = 10^{-3} - 10^{-1}$. The refined mesh with inflations to the walls, interfaces and injected particles have been generated. The pressure, velocity and shear stress fields in the tube have been computed. The sample spherical elastic particles with $d = 0.05$ mm (smaller embryos) and $d = 0.1$ mm (larger embryos) have been located in the middle section of the liquid column (Fig. 6) at the radial coordinates $r/R = 0; 0.25; 0.5; 0.75$ (Fig. 7) and their trajectories have been computed.

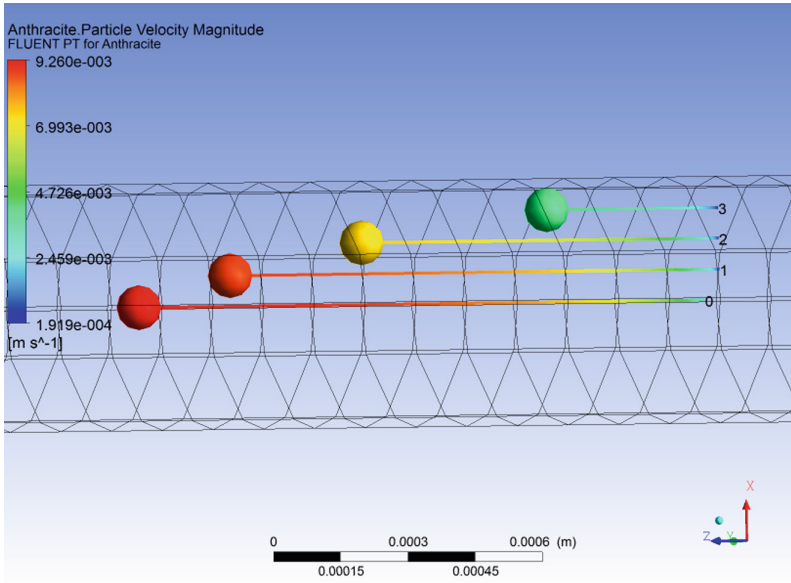


Fig. 7. Velocities of four sample particles at the time $t = 2$ s.

5 Results

One of the most useful approaches for the cell damage estimation is computation of the history of the damaging factors (pressures, pressure oscillations, shear stresses) during the cell movement [68–70]. It means, the listed factors must be computed along the trajectory of the sample particles in the tube. Some cells that move faster can experience higher mechanical forces onto their surfaces during a shorter travel time, while the cells that move at lower injection rates will experience the lower mechanical stresses during the longer time. In that way, the optimal injection speed with the lowest damage factor could be determined from the computer simulation data.

This approach has been validated for quantitative estimation of the red blood cell (RBC) damage in the apparatus of the extracorporeal circulation, through the stenosed mitral valve and valve prostheses. Various mathematical models have been used to correlate the mechanical forces and exposure time to the degree of the RBC damage. The most popular models are (i) average shear stress model [70], (ii) temporal differential model [71], and (iii) total differential model [72].

Based on this approach, the non-dimensional damage accumulation factor (DAF) can be computed by a simple formula

$$\text{DAF} = \frac{1}{\text{IT} \cdot \Sigma \tau_*} \int_0^{\text{IT}} \int_{\Sigma} \sqrt{\tau_{12}^2 + \tau_{13}^2 + \tau_{23}^2} d\Sigma dt, \quad (4)$$

where Σ is the surface of the particle, τ_* is the critical dimensionless shear stress factor (at $\tau > \tau_*$ the surface of the particle will be damaged), τ_{ik} are the components of the shear stress tensor computed at the surface of the particle.

For the more detailed quantitative estimations of the damage, the integrals of normal forces (pressures), pressure oscillations, and deformations of surface may be included into DAF with corresponding weighting coefficients. As the threshold value the critical wall shear stress $\tau_* \sim 120$ mPa for mouse embryos [73, 74] is used here.

DAF computations have been carried out by gradual iterations with different time steps Δt for different injection speeds and data collection on τ_{ik} at each time step. When the particles were located closer to the wall of the tube, the shear stresses at their sides were non-symmetrical due to the parabolic-type flow profile of the fluid. This asymmetry generates rotation of the particle in the direction to the wall that produces the Magnus forces governing the particle towards the axis of the tube. In the concentrated suspensions such motion is suppressed by the repulsive forces, while in the case of single embryos there are no returning forces and the motion of the particles is more complex.

The computed DAF values are presented in Fig. 8a,b. The solid straight line corresponds to the damage threshold τ_* . As it follows from the results, the very slow injection produces low shear stresses which might be slightly over the critical value due to longer travel time, but for the computed values $T = 83$ s the increase is very small (DAF = 1.04). The faster injection produces higher DAF indexes DAF ~ 1.4 that might be very influencing for the embryos. Based on the interpolations of the DAF values computed for three injection velocities, the safe regions of injection can be found for different embryo diameters. Since, location of the particle along the radius of the tube is unpredictable, the worst case with $r/R = 0.5$ must be chosen. It gives us optimal injection velocities $U_{\text{ing}} \sim 3\text{--}6$ mm/s for the smaller particles, that gives DAF = 0.85 and IT = 18–27 s. For the bigger embryos the injection velocities $v \sim 4\text{--}6$ mm/s that gives DAF ~ 0.95 and IT = 18–21 s can be recommended.

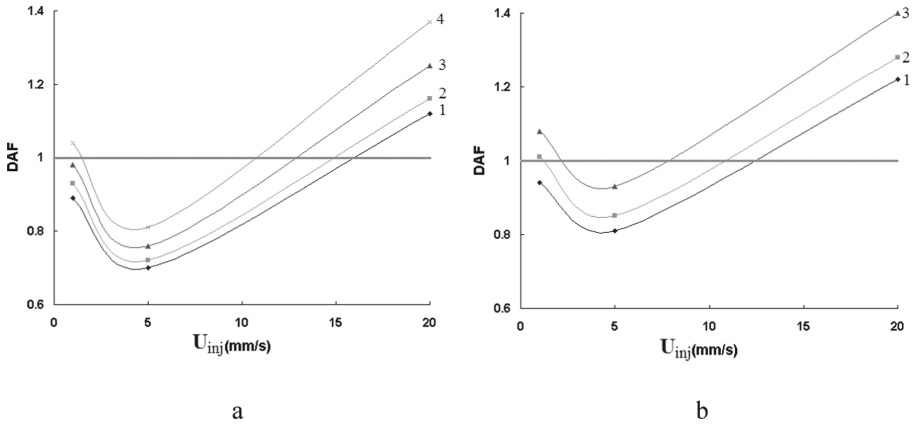


Fig. 8. Dependences $DAF(U_{inj})$ computed for the particles with $d = 0.2$ mm (a) and $d = 0.1$ mm (b); the curves 1–4 correspond to $r/R = 0; 0.25; 0.5; 0.75$.

6 Conclusions

The literature review revealed the following biomechanical aspects of the IVT procedure:

- 1) Viscoelastic properties of the 4–6 day old embryos [3, 19, 22, 31, 75];
- 2) Existence of the peristaltic waves and oscillatory fluid dynamics [34–42];
- 3) Catheter shape and tip location [55–61];
- 4) Ejection speed and duration of the procedure [62, 63];
- 5) Fluid composition and viscosity [55, 64];
- 6) Importance of the individualized procedure based on preliminary mathematical modeling and artificial intelligence approaches [76].

The steady viscous flow of three columns of the Embryo-Glue fluid with the embryo inside the middle column separated from a preceding and following columns by air bubbles of given volumes through a circular tube is studied. This problem has never been studied before in application to the ET procedure. The material parameters of the fluids, elasticity and damage shear stress values have been taken from published experimental data on zebra fish, mouse, and human embryos. A series of computational sets for three injection velocities, two embryo sizes and four initial locations of the particles have been obtained. The velocity fields, pressure distributions, pathlines and shear stresses have been computed. The mean and maximal values of the hydrodynamical parameters strongly depend on the injection velocity, particle size and location according to the tube's wall. The obtained results are in qualitative correspondence with experimental and CFD results [49, 50, 65, 66] obtained on the massless particles and small rigid particles in the tubes with rigid straight and waved surfaces.

A novel DAF parameter for estimation of the optimal patient-specific injection speed based on known size, elastic parameters and developmental stage of the embryo is proposed. The DAF is computed as the shear stress experienced by the embryo's surface embryo during its injection. The approach is well known and validated for the RBC

damage in the extracorporeal systems, valve prostheses or stenosed/calcified valves. For the ET procedure the approach has not been studied yet. It was shown, the numerical computations for three different injection velocities gives enough data for the interpolation of the dependencies $DAF(U_{inj})$ and estimation the limits for optimal U_{inj} for known embryo size and properties. Fast injection may produce high DAF due to high shear stresses especially when the embryo is closer to the wall, while the slow injection may also give higher DAF values due to longer IT of the embryo even at the low shear stress conditions.

The obtained results are based on an oversimplified elastic model of the embryo and the values measured on the mouse blastocysts only. More reliable data can be obtained on the realistic viscoelastic models of the embryo. The computed results also need validation by the experiments on human embryos. Other potential damaging factors (pressures, pressure gradients, variations in time, deformation of surfaces, etc.) can also be accounted for in (4) that will be done in future studies.

References

1. WebMD. <https://www.webmd.com/infertility-and-reproduction/guide/in-vitro-fertilization>
2. Krupinski P., Chickarmane, V., Peterson, C.: Simulating the mammalian blastocyst - molecular and mechanical interactions pattern the embryo. *Comput. Biol.* **7**(5), e1001128 (2011)
3. Yanez, L.Z., Camarillo, D.B.: Microfluidic analysis of oocyte and embryo biomechanical properties to improve outcomes in assisted reproductive technologies. *Mol. Hum. Reprod.* **23**(4), 235–247 (2017)
4. Huang, S., Ingber, D.E.: The structural and mechanical complexity of cell-growth control. *Nat. Cell Biol.* **1**, E131–E138 (1999)
5. Chicurel, M.E., Chen, C.S., Ingber, D.E.: Cellular control lies in the balance of forces. *Curr. Opin. Cell Biol.* **10**, 232–239 (1998)
6. Janmey, P.A.: The cytoskeleton and cell signaling: component localization and mechanical coupling. *Physiol. Rev.* **78**, 763–781 (1998)
7. Wang, J.H.-C., Thampatty, B.P.: An introductory review of cell mechanobiology. *Biomech. Model Mechanobiol.* **5**, 1–16 (2006)
8. Huang, A.H., Farrell, M.J., Kim, M., Mauck, R.L.: Long-term dynamic loading improves the mechanical properties of chondrogenic mesenchymal stem cell-laden hydrogels. *Eur. Cells Mater.* **19**, 72–85 (2010)
9. Engler, A.J., Sen, S., Sweeney, H.L., Discher, D.E.: Matrix elasticity directs stem cell lineage specification. *Cell* **126**, 677–689 (2006)
10. Suresh, S., et al.: Connections between single-cell biomechanics and human disease states: gastrointestinal cancer and malaria. *Acta Biomater.* **1**, 15–30 (2005)
11. Xu, W., et al.: Cell stiffness is a biomarker of the metastatic potential of ovarian cancer cells. *PLoS ONE* **7**, e46609 (2012)
12. Batyuk, L., Kizilova, N.: Modeling of dielectric permittivity of the RBC membrane as a three-layer model. In: *Development trends in Medical Science and Practice*, pp. 18–37. Baltija Publishing, Riga (2018). <https://doi.org/10.30525/978-9934-571-31-2>
13. Batyuk, L., Kizilova, N.: Dielectric properties of red blood cells for cancer diagnostics and treatment. *AS Cancer Biol.* **2**(10), 55–60 (2018)
14. Foo, J.Y., Lim, C.S.: Biofluid mechanics of the human reproductive process: modelling of the complex interaction and pathway to the oocytes. *Zygote* **16**, 343–354 (2008)

15. Muglia, U., Motta, P.M.: A new morpho-functional classification of the Fallopian tube based on its three-dimensional myoarchitecture. *Histol. Histopathol.* **16**, 227–237 (2001)
16. Kim, M.S., Bae, C.Y., Wee, G., Han, Y.M., Park, J.K.: A microfluidic in vitro cultivation system for mechanical stimulation of bovine embryos. *Electrophoresis* **30**, 3276–3282 (2009)
17. Beebe, D., Wheeler, M., Zeringue, H., Walters, E., Raty, S.: Microfluidic technology for assisted reproduction. *Theriogenology* **57**, 125–135 (2002)
18. Swain, J.E., Smith, G.D.: Advances in embryo culture platforms: novel approaches to improve preimplantation embryo development through modifications of the microenvironment. *Hum. Reprod. Update.* **17**, 541–557 (2011)
19. Wheeler, M.B., Walters, E.M., Beebe, D.J.: Toward culture of single gametes: the development of microfluidic platforms for assisted reproduction. *Theriogenology* **68**, S178–S189 (2007)
20. Krisher, R.L., Wheeler, M.B.: Towards the use of microfluidics for individual embryo culture. *Reprod. Fertil. Dev.* **22**, 32 (2010)
21. Lai, D., Smith, G.D., Takayama, S.: Lab-on-a-chip biophotonics: its application to assisted reproductive technologies. *J. Biophotonics.* **5**, 650–660 (2012)
22. Hwang, H., Lu, H.: Microfluidic tools for developmental studies of small model organisms—nematodes, fruit flies, and zebrafish. *Biotechnol. J.* **8**, 192–205 (2013)
23. Khalilian, M., Navidbakhsh, M., Valojerdi, M.R., Chizari, M., Yazdi, P.E.: Estimating Young's modulus of zona pellucida by micropipette aspiration in combination with theoretical models of ovum. *J. R. Soc. Interface* **7**, 687–694 (2010)
24. Dean, J.: Biology of mammalian fertilization: the role of the zona pellucida. *J. Clin. Invest.* **89**, 1055–1059 (1992)
25. Green, D.P.L.: Three-dimensional structure of the zona pellucida. *Rev. Reprod.* **2**, 147–156 (1997)
26. Liu, X., Fernandes, R., Jurisicova, A., Casper, R.F., Sun, Y.: In situ mechanical characterization of mouse oocytes using a cell holding device. *Lab. Chip.* **10**, 2154–2161 (2010)
27. Murayama, Y., et al.: Omata Mouse zona pellucida dynamically changes its elasticity during oocyte maturation, fertilization and early embryo development. *Human Cell* **19**, 119–125 (2006)
28. Murayama, Y., et al.: Elasticity measurement of zona Pellucida using a micro tactile sensor to evaluate embryo quality. *J. Mamm. Ova. Res.* **25**, 8–16 (2008)
29. Khalilian, M., Navidbakhsh, M., Valojerdi, M.R., Chizari, M., Yazdi, P.E.: Alteration in the mechanical properties of human ovum zona pellucida following fertilization: experimental and analytical studies. *Exp. Mech.* **51**, 175–182 (2011)
30. Liu, X., Shi, J., Zong, Z., Wan, K.-T., Sun, Y.: Elastic and viscoelastic characterization of mouse oocytes using micropipette indentation. *Ann. Biomed. Eng.* **40**(10), 2122–2130 (2012)
31. Moendarbary, E., Valon, L., Fritzsche, M., et al.: The cytoplasm of living cells behaves as a poroelastic material. *Nature* **12**(3), 253–261 (2013)
32. Liu, X., Kim, K., Zhang, Y., Sun, Y.: NanoNewton force sensing and control in microrobotic cell manipulation. *Int. J. Robot. Res.* **28**, 1065–1076 (2009)
33. Yanez, L.Z., Han, J., Behr, B.B., Pera, R.A.R., Camarillo, D.B.: Human oocyte developmental potential is predicted by mechanical properties within hours after fertilization. *Nature Commun.* **7**, 10809 (2016)
34. Fauci, L.J., Dillon, R.: Biofluidmechanics of reproduction. *Annu. Rev. Fluid Mech.* **38**, 371–394 (2006)
35. Osada, H., Tsunoda, I., Matsuura, M., Satoh, K., Kanayama, K., Nakayama, Y.: Investigation of ovum transport in the oviduct: the dynamics of oviductal fluids in domestic rabbits. *J. Int. Med. Res.* **27**, 176–180 (1999)
36. Anand, S., Guha, S.K.: Mechanics of transport of the ovum in the oviduct. *Med. Biol. Eng. Comput.* **16**, 256–261 (1998)

37. Paltieli, Y., Weichselbaum, A., Hoffman, N., et al.: Laser scattering instrument for real time in-vivo measurement of ciliary activity in human fallopian tubes. *Hum. Reprod.* **10**, 1638–1641 (1995)
38. Misra, J.C.: *Biomathematics: Modelling and Simulation*. World Scientific (2006)
39. Leng, Z., Moore, D.E., Mueller, B.A., Critchlow, C.W., Patton, D.L., et al.: Characterization of ciliary activity in distal Fallopian tube biopsies of women with obstructive tubal infertility. *Hum. Reprod.* **11**, 3121–3127 (1998)
40. Montenegro-Johnson, Th.D., Smith, A.A., Smith, D.J., Loghin, D., Blake, J.R.: Modelling the fluid mechanics of cilia and flagella in reproduction and development. *Eur. Phys. J. E* **35**, 111 (2012)
41. Isachenko, V.: In-vitro culture of human embryos with mechanical micro-vibration increases implantation rates. *Reprod. BioMed. Online* **22**, 536–544 (2011)
42. Ezzati, M., Djahanbakhch, O., Arian, S., Carr, B.R.: Tubal transport of gametes and embryos: a review of physiology and pathophysiology. *J. Assist. Reprod. Genet.* **31**, 1337–1347 (2014)
43. Eytan, O., Elad, D.: Analysis of intra-uterine fluid motion induced by uterine contractions. *Bull. Math. Biol.* **61**(2), 221–238 (1999)
44. Li, M.J., Brasseur, J.G.: Nonsteady peristaltic transport in finite-length tubes. *J. Fluid Mech.* **248**, 129–151 (1993)
45. Mernone, A.V., Mazumdar, J.N., Lucas, S.K.: A mathematical study of peristaltic transport of a Casson fluid. *Math. Comp. Model.* **35**, 895–912 (2002)
46. Eytan, O., Jaffa, A.L., Elad, D.: Peristaltic flow in a tapered channel: application to embryo transport within the uterine cavity. *Med. Eng. Phys.* **23**, 473–482 (2001)
47. Blake, J.R., Vann, P.G., Winet, H.: A model of ovum transport. *J. Theor. Biol.* **102**, 145–166 (1983)
48. Verdugo, P., Lee, W., Halbert, S., Blandau, R., Tam, P.: A stochastic model for oviductal egg transport. *Biophys. J.* **29**, 257–270 (1980)
49. Aranda, V., Cortez, R., Fauci, L.: Stokesian peristaltic pumping in a three-dimensional tube with a phase-shifted asymmetry. *Phys. Fluids.* **23**, 081901–081910 (2011)
50. Aranda, V., Cortez, R., Fauci, L.: A model of Stokesian peristalsis and vesicle transport in a three-dimensional closed cavity. *J. Biomech.* **48**, 1631–1638 (2015)
51. Levi Setti, P.E., Albani, E., Cavagna, M., Bulletti, C., Colombo, G.V., Negri, L.: The impact of embryo transfer on implantation - a review. *Placenta* **24**(Suppl.B), S20–26 (2003)
52. Sadeghi, M.R.: The 40th anniversary of IVF: has art's success reached its peak? *J. Reprod. Infertil.* **19**(2), 67–68 (2018)
53. Lauko, I.G., Rinaudo, P., Dashev S.: A computational parameter study of embryo transfer. *Ann. Biomed. Eng.* **35**(4), 659–671 (2007)
54. van Weering, H.G., Schats, R., McDonnell, J., Vink, J.M., Vermeiden, J.P., Hompes, P.G.: The impact of the embryo transfer catheter on the pregnancy rate in IVF. *Hum. Reprod.* **17**, 666–670 (2002)
55. Eytan, O., Zaretsky, U., Jaffa, A.J., Elad, D.: In vitro simulations of embryo transfer in a laboratory model of the uterus. *J. Biomech.* **40**, 1073–1080 (2007)
56. Lambers, M.J., Dogan, E., Kosteljik, H., Lens, J.W., Schats, R., Hompes, P.G.: Ultrasonographic-guided embryo transfer does not enhance pregnancy rates compared with embryo transfer based on previous uterine length measurement. *Fertil. Steril.* **86**, 867–872 (2006)
57. Mansour, R.T., Aboulghar, M.A.: Optimizing the embryo transfer technique. *Hum. Reprod.* **17**, 1149–1153 (2002)
58. Frankfurter, D., Trimarchi, J.B., Silva, C.P., Keefe, D.L.: Middle to lower uterine segment embryo transfer improves implantation and pregnancy rates compared with fundal embryo transfer. *Fertil. Steril.* **81**, 1273–1277 (2004)

59. Tiras, B., Polat, M., Korucuoglu, U., Zeyneloglu, H.B., Yarali, H.: Impact of embryo replacement depth on in vitro fertilization and embryo transfer outcomes. *Fertil. Steril.* **94**, 1341–1345 (2010)
60. Rovei, V., et al.: IVF outcome is optimized when embryos are replaced between 5 and 15 mm from the fundal endometrial surface: a prospective Yanez e analysis on 1184 IVF cycles. *Reprod. Biol. Endocrinol.* **11**, 114 (2013)
61. Cenksoy, P.O., Fıçıcıoğlu, C., Yesiladali, M., Akcin, O.A., Kaspar, C.: The importance of the length of uterine cavity, the position of the tip of the inner catheter and the distance between the fundal endometrial surface and the air bubbles as determinants of the pregnancy rate in IVF cycles. *Eur. J. Obstet. Gynecol. Reprod. Biol.* **172**, 46–50 (2014)
62. Caanen, M.R., et al.: Hompes embryo transfer with controlled injection speed to increase pregnancy rates: a randomized controlled trial. *Gynecol. Obstet. Invest.* **81**, 394–404 (2016)
63. Groeneveld, E., et al.: Standardization of catheter load speed during embryo transfer: comparison of manual and pump-regulated embryo transfer. *Reprod. Biomed. Online* **24**(2), 163–169 (2012)
64. Schoolcraft, W.B.: Importance of embryo transfer technique in maximizing assisted reproductive outcomes. *Fertil. Steril.* **105**(4), 855–860 (2016)
65. Bilalis, D., et al.: Use of different loading techniques for embryo transfer increasing the risk of ectopic pregnancy. *Hum. Reprod. (Abstract Book, P-479)* **17**, 162 (2002)
66. Yaniv, S., Elad, D., Jaffa, A.J., Eytan, O.: Biofluid aspects of embryo transfer. *Ann. Biomed. Eng.* **31**, 1255–1262 (2003)
67. Feng, J.Q.: A long gas bubble moving in a tube with flowing liquid. *Int. J. Multiph. Flow* **35**, 738–746 (2009)
68. Leverett, L.B., et al.: Red blood cell damage by shear stress. *Biophys. J.* **12**(3), 257–273 (1972)
69. Parfitt, H.S., Davies, S.V., Tighe, P., Ewings, P.: Red cell damage after pumping by two infusion control devices (Arcomed VP 7000 and IVAC 572). *Transfus. Med.* **17**(4), 290–295 (2007)
70. Wilson, A.M.M.M., Peterlini, M.A.S., Pedreira, M.L.G.: Infusion pumps and red blood cell damage in transfusion therapy: an integrative revision of the academic literature. *Rev. Latino-Am. Enfermagem.* **24**, e2763 (2016). <https://doi.org/10.1590/1518-8345.1155.2763>
71. Goubergrits, L., Affeld, K.: Numerical estimation of blood damage in artificial organs. *Artif. Organs* **28**(5), 499–507 (2004)
72. Yeleswarapu, K.K., et al.: A mathematical model for shear-induced hemolysis. *Artif. Organs* **19**(7), 576–582 (1995)
73. Xie, Y., Wang, F., Zhong, W., et al.: Shear stress induces preimplantation embryo death that is delayed by the zona pellucida and associated with stress-activated protein kinase mediated apoptosis. *Biol. Reprod.* **75**, 45–55 (2006)
74. Kizilova, N., Batyuk, L., Baranets, V.: Human red blood cell properties and sedimentation rate: a biomechanical study. In: Arkusz, K., Będziński, R., Klekiel, T., Piszczatowski, S. (eds.) *BIOMECHANICS 2018. AISC*, vol. 831, pp. 3–22. Springer, Cham (2019). https://doi.org/10.1007/978-3-319-97286-2_1
75. Elad, D., Jaffa, A.J., Grisaru, D.: Biomechanics of early life in the female reproductive tract. *Physiology* **35**, 134–143 (2020)
76. Xi, Q., Yang, Q., Wang, M., et al.: Individualized embryo selection strategy developed by stacking machine learning model for better in vitro fertilization outcomes: an application study. *Reprod. Biol. Endocrinol.* **19**(1), 53 (2021)